Utility of Satellite Remote Sensing for Land-Atmosphere Coupling and Drought Metrics.

*Joshua K. Roundy[1] and Joseph A. Santanello[2]

Journal of Hydrometeorology

Submission July 2016

[1]Department of Civil, Environmental, and Architectural Engineering, University of Kansas, Lawrence, Kansas

[2] Hydrological Sciences Laboratory, Goddard Space Flight Center, Greenbelt, Maryland

*Corresponding Author:
Joshua K. Roundy
Department of Civil, Environmental, and Architectural Engineering
University of Kansas
Lawrence, Kansas
jkroundy@ku.edu

Key words: Land-atmosphere interactions, remote sensing, drought

Abstract

Feedbacks between the land and the atmosphere can play an important role in the water cycle and a number of studies have quantified Land-Atmosphere (L-A) interactions and feedbacks through observations and prediction models. Due to the complex nature of L-A interactions, the observed variables are not always available at the needed temporal and spatial scales. This work derives the Coupling Drought Index (CDI) solely from satellite data and evaluates the input variables and the resultant CDI against in-situ data and reanalysis products. NASA's AQUA satellite and retrievals of soil moisture and lower tropospheric temperature and humidity properties are used as input. Overall, the AQUA-based CDI and its inputs perform well at a point, spatially, and in time (trends) compared to in-situ and reanalysis products. In addition, this work represents the first time that in-situ observations were utilized for the coupling classification and CDI. The combination of in-situ and satellite remote sensing CDI is unique and provides an observational tool for evaluating models at local and large scales. Overall, results indicate that there is sufficient information in the signal from simultaneous measurements of the land and atmosphere from satellite remote sensing to provide useful information for applications of drought monitoring and coupling metrics.

1. Introduction

In the absence of strong advective influences, land-atmosphere (L-A) coupling (Seneviratne et al. 2010) drives the diurnal cycle of clouds and precipitation that can greatly impact the water cycle. As a result, there has been a great deal of work to quantify L-A interactions and feedbacks through observations and prediction models. Much of this work has been carried out by the Global Energy and Water Exchanges Project (GEWEX) Global Land/Atmosphere System Study (GLASS) local land-atmosphere coupling (LoCo; Santanello et al. 2011) working group. As part of this work a suite of diagnostics has been developed, ranging in applicability from observations to models and spanning a broad range of spatiotemporal scales (Ferguson and Wood 2011; Lintner et al. 2014; Dirmeyer et al. 2014; Tawfik et al. 2015). For example, mixing diagrams (Betts 1992; Santanello et al. 2009; Stommel 1947) are recommended to analyze entrainment into clouds and boundary layer processes at a point scale. In contrast, the rainfall triggering feedback strength (TFS) of (Findell et al. 2011) quantifies how rainfall frequency changes with surface evaporative fraction and requires model data over a period of 90-days or longer. Perhaps most well-known is the model-based coupling strength of the Global Land Atmosphere Coupling Experiment (GLACE) (Koster et al. 2006): coherence among members (Ω) is computed for two model ensembles - one with prescribed soil moisture and the other with freely evolving soil moisture - and the difference ($\Delta\Omega$) is deemed the coupling strength. The overall applicability of these respective L-A coupling metrics is inherently limited by the ability to observe the variables required by each, which for most remains only at the point scale or during short term field experiments due to the simultaneous soil moisture, surface flux, boundary layer, and precipitation measurement requirements.

62 Satellite data offers the ability to obtain some of these variables globally and routinely
63 (and thus has the most promise for GCM and model development applications), but has been
64 limited to date (Ferguson and Wood 2011; Roundy et al. 2013a; Taylor et al. 2012). In order to
65 make satellite observations useful for informing and improving the L-A interactions with in the
66 models requires further development of satellite-based metrics. The Coupling Drought Index
67 (CDI) developed by Roundy et al. (2013a), is such a metric since it has application to L-A
68 interactions and drought and can be calculated entirely from satellite remote sensing. The CDI is
69 based on a classification of L-A interactions into regimes built off of the work of Findell and
70 Eltahir (2003a,b), who demonstrated the preferential tendency for convective rainfall over wet
71 (i.e., wet-advantage) versus dry soils (i.e., dry advantage), depending on low-level atmospheric
72 humidity (HI) and instability (i.e., convective triggering potential, CTP). The CTP is a measure
73 of atmospheric stability defined as the area between the temperature profile and a moist adiabat
74 from 100 mb to 300 mb above the surface. The HI is a measure of low-level boundary layer
75 moisture given by the sum of the dew point depression at 50mb and 150 mb above the surface.
76 Thus, the regimes are strictly a function of lower troposphere temperature profiles and moisture
77 condition.
78 The two dimensional space comprised of the CTP and HI relationship can then be
79 classified into regimes based on the ability of the soil moisture (SM) state to initiate convection
80 (Findell and Eltahir 2003b). Later work by Ferguson and Wood (2011) applied this classification
81 approach to different datasets and regions, and showed that the classified space presented by
82 Findell and Eltahir was too stringent. Roundy et. al (2013a) developed a method of using local
83 statistics of top layer soil moisture to classify the wet-advantage and dry-advantage sub-spaces
84 within the CTP-HI space regionally. This approach separates the CTP-HI space into bins and

uses the Two-Sample Kolmogorov–Smirnov to compare the distribution of SM in each bin against the climatological SM. Bins of the CTP–HI space with predominantly wetter soils are considered wet coupling and bins that are predominantly drier are dry coupling. Bins that are neither dry nor wet (in a climatological sense) are classified transitional and bins with few samples are considered atmospherically controlled. The rational for this approach is that there is an inherent connection between the soil moisture and heat flux partitioning that causes a persistence into the dry and wet coupling regimes that is driven by the feedback between the land and the atmosphere. Due to the sensitivity of bin size and the significance level of the KS test, the classification uses an ensemble approach where each ensemble member utilizes a different bin size and significance level. This accounts for the sensitivity of these classification parameters and provides a means to quantify the uncertainty. The final discrete classification is determined based on the uncertainty in each bin (see Roundy et al. (2013a) for more details). Although there is similarity between the Findell and Eltahir (2003b) and Roundy et al. (2013a) classification, the latter is based on soil moisture and includes days with *and* without convective precipitation. To denote this difference, the regime names in Roundy et al. are referred to simply as 'dry coupling' and 'wet coupling' to indicate the persistent nature of the overall dry and wet events, respectively.

A schematic of the three variables used in the classification (CTP, HI, and SM) and the classified CTP-HI space for a grid cell in the Southern Great Plains (SGP) using the MERRA reanalysis is given in Fig. 1a. As illustrated in Fig. 1a, the CTP is calculated by integrating the area between the moist adiabat and the temperature profile. The CTP in Fig. 1a is positive and indicates an unstable atmosphere. If the moist adiabat is cooler than the temperature profile, then the CTP is negative and indicates a stable atmosphere. The HI is a measure of the atmospheric

humidity and is calculated as the sum of the dew point depression at 50 and 150 mb above the surface. A large value of HI, as shown in Fig 1a, is indicative of a dry atmosphere. As the dew point temperature approaches the temperature profile, the atmosphere moves closer to saturation and the HI decreases. A climatological sample of daily CTP, HI and SM are then used to create the classification of the CTP-HI space. To do this the CTP-HI space is broken up into bins and each is classified based on the soil moisture values that fall into that bin by the method described above. Once the CTP-HI space is classified it is used to generate a daily coupling classification based on the location of the CTP and HI for that day. For example, given the classified CTP-HI space in Fig. 1, a day with CTP of 400 J/kg and a HI of 30° C would be classified as dry coupling.

Multiple days with the same coupling classification are considered to be an event and are called dry or wet coupling events. These events can persist for days to weeks. An example of a persistent dry and wet coupling event that occurred in the same year (2000) for a grid cell in the SGP is given in Fig. 1b based on the MERRA reanalysis. Vertical dashed lines denote the beginning and ending of the event as determined by the daily classification, where the start of the event is the first day with a daily classification of dry or wet coupling respectively and the end of the event is the last day of the consistent daily classification of dry or wet coupling. Persistent events, such as those depicted in Fig. 1b, can have large impacts the local water and energy cycle. To demonstrate this, timeseries of daily average SM, Evaporative Fraction (EF, ratio of latent heat flux to available energy), Boundary Layer Height (BLH), the Lifting Condensation Level (LCL, the level to which a parcel of air can be lifted adiabatically before it becomes saturated) deficit (difference between the LCL and BLH) and the nighttime and daytime precipitation are also included. The dry coupling event is typified by low soil moisture, a small

surface EF, a large boundary layer height and a large LCL deficit. Toward the end of the dry coupling event the BLH increases and the LCL deficit decreases due to an increase in BLH. In contrast, the wet coupling event has high soil moisture, a large EF, small BLH and a small LCL deficit. The wet coupling event also shows a decrease in the LCL towards the end of the event, however BLH also decreases which indicates that the decrease in the LCL deficit is due to a decrease in the LCL due to the large latent heat flux. Daytime precipitation occurs during both dry and wet coupling events, however, the precipitation is less frequent and of a smaller in magnitude during the dry coupling event. Although the persistence in these coupling regimes can be explained by L-A feedbacks, it is important to note that advected moisture into the region also plays a key role (Song et al. 2015) and any dry or wet coupling event is ultimately a combination of local feedback mechanism and large-scale circulation patterns.

The cumulative negative (dry coupling→drying) and positive feedback (wet coupling→ wetting) of these events is the foundation of the Coupling Drought Index (CDI), which is simply the number of dry coupling days minus the wet coupling days, divided by the total number of days over a period of time. CDI has a range from -1 (all wet coupling) to +1 (all dry coupling) and gives an average measure of coupling over the chosen time window. The CDI has been successfully applied in the evaluation of reanalysis and seasonal forecasts (Roundy et al. 2013a,b; Roundy and Wood 2014).

One of the unique characteristics of metrics based on the CTP, HI and SM is that these variables can be derived from simultaneous measurements from instruments onboard NASA's AQUA satellite. Specifically, the Atmospheric Infrared Sounder (AIRS) provides temperature and moisture profiles that can be used to estimate the CTP and HI while measurements from the Advanced Microwave Scanning Radiometer for EOS (AMSR-E) instrument can be used to

derive soil moisture. The simultaneous measurement of both land and atmospheric variables from the AQUA satellite provides a unique large-scale and observationally-based dataset for developing coupling metrics suited for evaluating weather and climate models. This work aims to assess the utility and uncertainty of the satellite data for application to the coupling classification. This is done by first introducing the in-situ, satellite and reanalysis datasets and methods utilized in this study (section 2). Next, a comparison of the measurements and the derived variables (CTP, HI and SM) across datasets is made (section 3.1) followed by an evaluation of utilizing these variables to the coupling classification and CDI in section 3.2. The CDI from remote sensing is then compared to other common surface and boundary layer variables from reanalysis in section 3.3 and is followed by discussion and conclusions in section 4.

2. Datasets and Methods

2.1 Datasets

In this work, four different datasets are used to calculate the CTP, HI and SM needed for the CDI classification and includes satellite remote sensing, reanalysis and in-situ data. Table 1 provides a summary of the datasets used, the type of data and temporal range of the dataset that was utilized in this study. The satellite remote sensing data is from the NASA AQUA satellite, which includes the Atmospheric Infrared Sounder (AIRS) as well as the Advanced Microwave Scanning Radiometer-EOS (AMSR-E). The AIRS data used in this study is from the Level 3 Version 6 data product and provides 12 vertical levels of consistent measurements of temperature and humidity (Susskind et al. 2011). These AIRS observations are provided twice daily at 1:30AM and 1:30PM local time on a 1° x 1° global grid from August 2002 to present. Only the 1:30 AM (descending overpass) data is used in this study, as it provides a better

177 measure of the atmosphere in early morning before the impact of the daytime surface heat fluxes.
178 These observations of atmospheric temperature and humidity enable the calculation of the CTP
179 and HI. The measurements from the Advanced Microwave Scanning Radiometer-EOS (AMSR-
180 E) aboard AQUA are used to derive soil moisture from the Land Surface Parameter Model
181 (LPRM) (Owe et al. 2008) and is representative of the top 2-cm soil layer. Unfortunately, the
182 AMSR-E instrument failed in 2011 and limits the availability of soil moisture data from 2002-
183 2011.

184 Reanalysis products are also used in this study as they provide global, continuous and
185 long-term records of the climate system constructed by combining observations and models.
186 Reanalysis data sets also provide a means for initializing forecasts models with the best
187 temporally and spatially continuous estimates of earth system variables for weather and climate
188 forecasts. It is important to remember that although reanalysis assimilates observations, there is
189 still a large component that is based on the parameterizations and assumptions inherent in the
190 model. Therefore, while reanalysis may assimilate a similar set of observations, they may
191 provide different representations of the climate due to the differences in the assimilation
192 technique and modeling.

193 Two different reanalysis datasets are considered, NASA's Modern-Era Retrospective
194 analysis for Research and Applications (MERRA; Rienecker et al. 2011) and the National
195 Centers for Environmental Prediction (NCEP) Climate Forecast System Reanalysis (CFSR; Saha
196 et al. 2010). These datasets were chosen due to their global coverage and availability. MERRA is
197 based on NASA's Goddard Earth Observing System (GEOS-5; Rienecker et al. 2011), which
198 utilizes the Catchment LSM (Koster et al. 2000). The top soil layer in Catchment represents the
199 uppermost 0–2cm layer. MERRA has a 0.5 x 0.667 degree horizontal resolution over the globe

200 with 72-layer vertical resolution and the assimilated data is provided at 6-hourly increments from
201 1979-present. CFSR includes the GFSv2 atmospheric component with 64-layers in the vertical
202 with a horizontal resolution of T382 (0.313°), a coupled ocean model MOM4 with 40 vertical
203 layers, and the Noah land surface model (Ek et al. 2003), which has four soil layers that cover 0-
204 10cm, 10-40cm, 40-100cm and 100-200cm respectively. Although CFSR has a T382 horizontal
205 resolution, the atmospheric data is archived at a 0.5° resolution, while the land surface data is
206 archived at the T382 resolution. The original CFSR has a record length from 1979 through
207 March of 2011, however in April 2011 an updated version of CFSv2 was put into operation to
208 produce real-time CFSR data through the present (Saha et al. 2014). These combined datasets
209 make up the whole of the CFSR data used in this study that provides 6-hourly analysis data from
210 1979 to present.

211 The last type of data utilized in this study is in-situ data and provides direct
212 measurements of the atmosphere and the land surface as part of the Department of Energy's
213 (DOE's) continuous record of observational data from ARM-SGP (covering a large part of OK
214 and KS). Because of this unique dataset that includes atmospheric and surface variables, the
215 SGP has been the test site for a number of studies (Santanello et al. 2013, 2015). Specifically,
216 radiosonde profiles (http://dx.doi.org/10.5439/1021460) and top layer soil moisture from the Soil
217 Water and Temperature Profiling System (SWATS; http://dx.doi.org/10.5439/1150274) from the
218 ARM central facility (36.610°N, 97.4899°W) near Lamont Oklahoma were utilized. The
219 SWATS provides 6 levels of soil moisture measurements for two soil profiles (east and west)
220 that are separated by a distance of 1 meter. Only the measurements at 5cm are utilized and are
221 calculated as the average of the two profile measurements. The radiosonde data provides high
222 vertical resolution measurements of atmospheric temperature and humidity that can be utilized

for calculating the CTP and HI. The radiosonde data is routinely collected four times a day at approximately 5:30, 11:30, 17:30 and 23:30 UTC and the soil moisture is collected hourly.

2.2 Methods

One of the challenges of comparing all the datasets is the different spatial resolution, domains and temporal ranges. To make consistent comparisons all the datasets are up-scaled to the 1° x 1° global grid of the AIRS data through bin averaging. To make a comparison to the SGP site (36.610°N, 97.4899°W), the containing grid cell (36.5°N, 97.5°W) from the 1° x 1° global grid of the AIRS is used. In addition to spatial differences, there is also a temporal inconsistency between the datasets. The AQUA satellite data is acquired around 1:30 AM (07:30 UTC) local time, where the reanalysis data is provided every 6 hours (00, 06, 12, 18 UTC) and the in-situ is also available approximately every six hours (05:30, 11:30, 17:30, 23:30 UTC) which is a 1.5 hour and 2-hour difference for the reanalysis and in-situ measurements respectively. To account for this difference in time, the SM and atmospheric profile data from in-situ and reanalysis are linearly interpolated to correspond with the satellite overpass. This temporal linear interpolation in time is done before calculating the CTP and HI. This temporal interpolation provides a reasonable estimate since the nighttime profiles of temperature and humidity are typically slowly varying in the early morning hours (e.g. 12:00-6:00 AM local time) in terms of their bulk structure in the lower troposphere, while SM evolves on much slower timescales overall.

These spatially and temporally consistent estimates of CTP, HI and SM are used to classify the CTP-HI space and give a daily coupling classification following the procedures outlined in Roundy et al. (2013a). Due to the spatial consistency of the coupling regimes, earlier work used all the grid cells in the entire Southeast United States for the classification (Roundy et

al. 2013a). While there is general consistency in the classification over regions with similar climate, a regional classification leads to abrupt spatial changes in when moving across regional boundaries. To overcome this limitation, Roundy et al. (2013b) included the local classification of each grid cell while maintaining regional consistency by utilizing the surrounding grids cells to provide a spatially consistent classification. As compared to utilizing the grid data only, incorporating the surrounding grid cells provides an increased sample size that leads to a robust ensemble that accounts for the uncertainty in the classification. This technique results in a classification with weakened spatial heterogeneity as compared to the raw atmospheric profiles and SM, but still represents the larger spatial patterns. This methodology of using the surrounding grid cells is used to provide the coupling classification for the reanalysis and remote sensing datasets.

As this is the first time that in-situ observations have been used in the classification methodology, the classification of point data presents some challenges. One major challenge is producing a unique classification for the in-situ data given the absence of surrounding grid cells to incorporate in the classification. One of the key aspects of the classification methodology is to quantify the uncertainty in the CTP-HI space by using an ensemble of bin sizes and significance levels. The ensemble parameters (i.e. number of bin sizes, significance levels and uncertainty thresholds) were developed by Roundy et al. (2013b) for gridded data that incorporate the nearest grid cells and have been used for a number of studies (Roundy et al. 2013b; Roundy and Wood 2014; Santanello et al. 2015; Song et al. 2015). Applying the ensemble parameters from the gridded data to a single point drowns out the signal due to the impact of small bin sizes and strict significant levels for the smaller sample size. To account for this difference in the in-situ data, a series of test were performed with the AQUA data to adjust the ensemble parameters to

achieve a consistent classification between utilizing a single grid cell only and the grid cell with the surrounding grid cells. This resulted in bin sizes ranging from 7-17 and significance levels from 10% to 15%, as compared to bins ranging from 10-35 and significance levels from 1% to 5%. The lower significance level indicates more uncertainty in the classification and that resulted in a point classification with a smaller regime classification. This is consistent with the results from Roundy et al. (2013a) that showed that a smaller sample size resulted in a consistent yet smaller regime classification. Notwithstanding the smaller regime classification, the point specific classification parameters yield a consistent classification and are used for the in-situ data.

To produce a unique classification that accounts for the characteristics of a dataset requires a training period that must be consistent across all the datasets due to the sensitivity of training period on the classification. The maximum consistent training period across all datasets is an 9-year period from 2003-2011. Although the classification of the CTP-HI space is only done for 2003-2011, the daily coupling classification only requires daily values of CTP and HI once the CTP-HI space is classified. Therefore, the analysis will focus on the full period of data availability from 2003-2015 for all datasets (see Table 1). In this sense the period from 2012-2015 acts as a cross validation period as the CDI is being applied for period that is different from the training period.

3. Results

3.1 Derived Variable Intercomparison

Observations from AQUA are first compared with in-situ measurements of the three variables used in the CDI, the CTP, HI and SM. A comparison of the atmospheric profiles of temperature and humidity (given as dew point temperature) for the in-situ observations and the

satellite data are given in Fig. 2 for a day in a dry year (2006) and wet year (2007) in the SGP. In comparing these datasets, the higher level of vertical detail in the radiosonde data is evident. Notwithstanding the low resolution in the vertical, the satellite profiles of atmospheric temperature show a good agreement with the in-situ observations. In contrast, the lack of vertical resolution in the satellite observations is more damaging in terms of dew point temperature. These characteristics directly translate to the CTP and HI. For the CTP, there is good agreement between the in-situ and satellite observations, with small relative differences. The HI on the other hand shows a larger disagreement between the in-situ and satellite observations due to the lack of vertical detail in the dew point temperature from AIRS. These results are consistent for both the dry and wet year. The number of observations in the CTP-HI range (50mb to 300mb above the surface) varies by day and location. For the examples shown in Fig. 2, the satellite observations have 3 and 2 measurements in the CTP-HI range compared to the 516 and 411 measurements from in-situ. This represents a substantial difference in the vertical that is noticeable in Fig. 2 and is likely one of the main causes for the discrepancy between the CTP and HI.

The above analysis only considers two days chosen at random during a dry and wet year, but comparing the CTP and HI over a larger time period and extending the comparison to include the comparison of in-situ observations with reanalysis can yield further insights. This comparison is given in Fig. 3 for the same location in the SGP but covering all available data from 2003-2015. For each variable, only days that have data from in-situ, satellite and reanalysis are shown in Fig. 3. This results in a CTP and HI comparison that includes data from 2003-2015, while the SM comparison only includes 2003-2011 due to the short record of AMSR-E data. For the CTP, the satellite observations show the largest scatter with in-situ observations with a Pearson and Spearman correlation of 0.71 and 0.78 as compared to 0.94 and 0.96 for MERRA

and 0.92 and 0.94 for CFSR. A similar relationship can be seen for the HI, with the reanalysis datasets showing a strong correlation with in-situ, while the satellite data shows much more scatter with a Pearson and Spearman correlation of 0.74 and 0.73. Although the two days shown in Fig. 2 indicate that the HI is dry compared to the in-situ observations , the regression line matches well with the one-to-one line with a slope of 0.97 and x-intercept of 1.26 that indicates that there is a wet bias (AQUA HI too low), particularly for the driest HI values from in-situ. The larger scatter between satellite CTP and HI and in-situ is likely due to the low resolution of the vertical levels from satellite that fails to capture the fine details (see Fig. 2).

Fig. 3c shows the in-situ SM at the ARM site compared against the AQUA/AMSR-E SM retrieval and the reanalysis products. The SM for each dataset is normalized by the maximum and minimum value (essentially resulting in a moisture availability) in order to account for the difference in the dynamic ranges of SM in each product. CFSR shows the highest correlation with in-situ SM with a Pearson and Spearman correlation of 0.66 and 0.69. MERRA and AQUA/AMSR-E SM have slightly lower correlations, of 0.58-0.63 and 0.56-0.6 respectively. Overall, the SM datasets show a greater spread and much lower correlations than the CTP or HI. There are three main reasons why the soil moisture data does not compare as well as the CTP and HI across the datasets. First, the inconsistency is likely partially due to the nature of soil moisture heterogeneity at a single site versus that of a large grid cell. While there is a similar difference in scale for the CTP and HI, the atmosphere is more homogeneous over the grid scale compared to the SM. Second, there are linear features present in the in-situ data that show little sensitivity to changes in SM from the reanalyses and satellite. This is a known limitation of the SWATS instrument where it is insensitive to soil moisture variations at certain thresholds (and is being rectified by the installation of new SM instruments at the SGP sites). The third reason for

the inconsistency is the difference in the depth of each of the measurements. The in-situ observations are at 5cm, while MERRA and AQUA cover the 0-2cm layer and CFSR covers the 0-10cm layer. This could be the reason that the CFSR matches better with the in-situ since the average point of the top-layer matches with the in-situ measurement. Notwithstanding the spatial scale, measurement errors and vertical difference in the measurements, there is still a reasonable amount of consistency that can capture larger regimes of SM that makes it useful application with the CDI.

3.2 Coupling Classification and CDI

This section extends the previous comparisons to the classification of the CTP-HI space and the CDI. As described above, the classification identifies areas in the two-dimensional space made up of the CTP and HI that have consistent statistics of soil moisture. Thus, the classified CTP-HI space is an integration of the three variables previously compared that identifies a connection or "coupling" of these variables. The classified CTP-HI space from in-situ, satellite and both reanalysis datasets is given in Fig. 4 for the SGP. All datasets show areas classified as dry coupling and wet coupling and show relative consistency between wet and dry coupling locations within the CTP-HI space. The in-situ classification has smaller regions of wet and dry coupling and a boxier shape due to the smaller sample size that necessitated and adjustment of the ensemble parameters as part of the classification algorithm.

The overlap of dry coupling and wet coupling regimes within the CTP-HI space with in-situ classification is quantified as the number of bins in the CTP-HI space with the same coupling regime classification as in-situ relative to the total number of bins defined as that coupling regime from the in-situ and given as a percentage. MERRA shows a consistency of 100% and 96% for wet and dry coupling respectively. CFSR has a consistency for both wet and

dry coupling at 100%. The AQUA classification is 82% consistent with in-situ classification for the wet coupling regime and 87% consistent for the dry coupling regime. Given this measure, there are two reasons that consistency could be less than 100%; first a difference in size of the regime space and second a difference in location. Given the small size of the in-situ regimes, the lower consistency between in-situ and satellite is due to the location, not the size. The AQUA classification shows a translation down the CTP dimension for both the wet and dry coupling regime. Consistency in wet coupling is highest for both MERRA and CFSR, which also have the highest correlation with in-situ data for CTP and HI. CFSR has the highest consistency with dry coupling and showed the highest correlation with SM. It is not surprising that the AQUA classification has a lower consistency with in-situ compared to the reanalysis, given the difference in the CTP, HI and SM shown in Fig. 3. Even though the difference in the location of the regimes results in a lower consistency for the AQUA dataset, the overall patterns across the datasets are comparable. This difference in the location of the coupling regimes in the CTP-HI space across datasets was one of the main reasons that a local-dataset specific classification of the CTP-HI space was developed by Roundy et al. (2013).

Although there are inconsistences among the datasets in terms of the coupling classification and the input, the coupling classification and resultant CDI are based on the temporal persistence in dry or wet coupling regime and it is arbitrary if the actual location of the regimes (i.e. in Fig. 4) are consistent. Furthermore, once the CTP-HI space is classified using the soil moisture data, only the CTP and HI are needed to produce a daily classification and calculate the CDI. This is particularly fortunate for the AQUA satellite and allows the calculation of the CDI beyond 2011 even though soil moisture data is no longer available. A comparison of the timeseries of the monthly CDI from 2003 to 2015 is given in Fig. 5a and shows consistency in

384 the temporal variability the datasets. This is partially due to the CDI capturing consistent
385 temporal relationships within coupling regimes that are not impacted by the inconsistencies
386 previously discussed.

387 Notwithstanding the consistency in the CDI among the datasets there are some noticeable
388 differences. First, the in-situ CDI has a lower magnitude than the reanalysis. This is particularly
389 noticeable for the extremely dry months (positive) and wet months (negative). This is likely due
390 to the smaller area classified as dry and wet coupling in the CTP-HI space (Fig. 4). The satellite
391 CDI magnitude is also smaller in amplitude as compared to reanalysis. This is consistent with
392 AQUA not being able to capture the extremes of HI (as discussed earlier). However, the satellite
393 and in-situ CDI does capture the relative peaks of dry (2011, 2012) and wet (2007) regimes well.
394 In comparing the two reanalysis datasets, CFSR has a higher CDI than MERRA for most
395 months. This is likely due to the larger boundary layer growth as a result of a persistent dry bias
396 in the PBL (Santanello et al. 2015).

397 The consistency between the CDI of the datasets is primarily seen in the summer months
398 (May-Sep), while the winter months generally have a low magnitude and there is more scatter
399 across the datasets. This is not surprising given the dominate nature of the coupling regimes in
400 the summer time. Since the summer months are more relevant to land-atmosphere interactions
401 and the CDI, the monthly CDI is compared in Fig. 5b for the summer months. The dark gray
402 points are for the training period (2003-2011) while the light gray points are from 2012-2015.
403 The overall correlations for reanalysis and satellite with in-situ CDI are significant at a 99%
404 confidence level across, with a Pearson and Spearman correlation of 0.85 and 0.83 for MERRA,
405 0.8 and 0.7 for CFSR and 0.68 and 0.68 for AQUA. There is also no noticeable degradation in
406 the relationship with the in-situ data outside of the training period. The relative rankings are

consistent with the previous analyses that examined the variables and classification that goes into the CDI (Fig. 3 and Fig. 4). Specifically, MERRA is more consistent with in-situ data at the SGP site, followed by CFSR and then AQUA.

Even though the MERRA reanalysis is more consistent with the in-situ data then the other datasets, it is important to remember that up to this point the analysis has only considered a single point and may or may not be representative of other locations. In fact, the ability to have observations over the globe is one of the major advantages of using satellite remote sensing to estimate the CDI. The CDI over the Contiguous United States is shown in Fig. 5c for MERRA, CFSR and AQUA for June of 2007. There is overall consistency across the datasets with the dominate spatial patterns evident in both reanalysis and satellite CDI and show the wet conditions in the Northwest, and the Southern Great Plains, as well as the drought in the intermountain region and in the Southeast. The spatial patterns are weaker for the satellite CDI, particularly for the magnitude and extent of the wet coupling area. Despite the weaker spatial patterns and limitations of the satellite data (vertical resolution, short record, course spatial scale), it still captures the primary signals and has potential to yield useful information as a large-scale observation.

3.3 CDI relationship to other variables

The CDI captures the intensification, persistence and recovery of drought through the persistence in the dry coupling and wet coupling regime. While it is clear from Fig. 1 that there is a connection between variables typically associated with L-A interactions and the coupling regimes, the relationships between CDI and these variables has never been quantified. Since these variables have different means and variance, each one is normalized to a standardized index by subtracting the mean and dividing by the standard deviation. In this manner, the CDI

from satellite remote sensing is compared with other L-A associated variables from reanalysis. The monthly-standardized anomalies of Precipitation (P), Total Soil Moisture (TSM), Daily Average Temperature (DAT) and Vapor Pressure Deficit (VPD), EF, BLH, CTP and HI are compared to the monthly anomaly of CDI. The correlations of the AQUA CDI with the aforementioned variables from MERRA and CFSR are given in the first two panels of Fig. 6 and the MERRA CDI compared to MERRA variables are given in panel three. Because AQUA itself is limited in terms of observing the majority of these individual variables, we compare AQUA CDI to the reanalysis products which are assumed to capture the bulk behavior of these coupling-related properties of the L-A system. Each panel includes the correlation of the spatial average standard anomaly for six climate regions (colors) and the entire U.S (grey and white boxes reflected around zero) for months in the May-Sep season (open shapes) and the full year (filled shapes).

For all three comparisons, the CDI and precipitation show a higher correlation in the western portion of the U.S. that only shows a minor increase during the summer months. The spatial difference in the correlation between the CDI and precipitation is less pronounced in the AQUA-CFSR comparison as compared to the AQUA-MERRA or MERRA-MERRA comparison. This suggests that the MERRA precipitation (which is known to have major limitations in timing and intensity over much of CONUS) may be the cause of this spatial difference. There is also less of a seasonal difference in the MERRA-MERRA comparisons, suggesting a greater seasonal difference in the AQUA CDI compared to MERRA. Total soil moisture shows a similar relationship with CDI and precipitation in that it has a higher correlation in the west and a relatively small seasonal difference. In fact, for the AQUA-MERRA and MERRA-MERRA comparison the correlations are nearly the same. This suggests that there

453 is a high correlation between precipitation and TSM in MERRA, as would be expected within
454 the same reanalysis system. In contrast, the AQUA-CFSR comparison for TSM shows a much
455 lower correlation and little spatial difference.

456 The daily average temperature and vapor pressure deficit show a higher correlation with
457 the CDI and a greater seasonal difference as compared to precipitation and soil moisture. The
458 AQUA CDI correlation with DAT and VPD nearly doubles during the summertime compared to
459 the full year and is more spatially homogeneous. The MERRA CDI and the MERRA VPD has
460 less of a seasonal difference in correlation and there is consistency in the correlation across the
461 different regions of the country, with a higher correlation in the west for both the DAT and VPD
462 that is consistent with P and TSM. This same relationship is weaker for AQUA-CFSR as
463 compared to AQUA-MERRA and MERRA-MERRA. This suggests a consistent spatial
464 relationship between the CDI and MERRA variables that may be a unique attribute to MERRA
465 and not CFSR.

466 The evaporative fraction has one of the lowest correlations with the CDI across all
467 comparisons and also shows little difference in the seasonal correlation. The CDI is not well
468 correlated with evaporative fraction for Midwest and especially the Northeast, while the highest
469 correlations are generally seen in the South and High Plains. BLH shows similar spatial patterns,
470 however CDI shows an overall higher correlation with BLH and an increase in the seasonal
471 variability as compared to the evaporative fraction. This indicates that the CDI is more strongly
472 correlated with the atmospheric side of L-A coupling and shows the greatest strength in the areas
473 that are considered hotspots (Koster et al. 2006). However, since the BLH is highly correlated
474 with the sensible heat flux, it may be that the energy cycle side of the land surface plays an
475 important role in the CDI evolution. The AQUA CDI is also more strongly correlated with the

476 BLH from CFSR compared to MERRA BLH, which is consistent with Santanello et al. (2015)
477 who found the MERRA BLH to be underestimated and lacking sensitivity to extremes.
478 The correlation of the CDI to the CTP and HI is among the strongest and is not surprising
479 given that the CTP and HI are used to derive the CDI. The CTP has a larger seasonal difference
480 in its correlation to the CDI as compared to the HI. In contrast the HI shows more spatial
481 variability in its correlation with the CDI. Overall the satellite based CDI shows slightly lower
482 correlations with other reanalysis variables then those seen internally within the MERRA
483 reanalysis. This is not surprising given that reanalysis variables should be more consistent, while
484 the satellite observations are more independent.

485 **4. Discussion and Conclusions**

486 The aim of this study is to assess the utility of CDI-based variables and metrics derived
487 from satellite remote sensing for global applications by comparing them with in-situ observations
488 and reanalysis datasets. Overall, the AQUA CDI performs well at a point, spatially, and in time
489 (trends) compared to in-situ and reanalysis products. This is especially promising given the
490 inherent limitations in vertical profile resolution and soil moisture retrieval, as advances in
491 satellite-based profiles (e.g. improved AIRS retrievals) and soil moisture retrievals (e.g. SMAP)
492 will provide improved estimates of L-A and CDI related quantities in the future. The satellite
493 observations of atmospheric temperature and humidity profiles and the derived metrics compare
494 well with in-situ observations, although differences exist, mainly due to the limitation of vertical
495 resolution of the satellite data (Fig. 2).
496 Although the lower vertical resolution of the atmospheric satellite data resulted in lower
497 correlations of the CTP and HI from satellite with in-situ data, the satellite data has sufficient
498 correlation with in-situ data to capture the main signal (Fig. 3). Both reanalysis datasets show an

equally strong correlation with the in-situ observations for CTP and HI, while the satellite data shows a lower correlation with in-situ HI as compared to the CTP. It should be noted that to date there has been very little focus or evaluation of AIRS L3 profile retrievals over land due to inherent difficulties in retrieving lower troposphere and PBL thermodynamics (due to factors such as limited weighting functions and surface emissivity; Susskind pers. communication). Moisture retrieval is inherently more difficult than temperature, and thus the results are not unexpected in that temperature (and CTP) performs better than moisture (and HI) against this small sample. The AIRS support product (L2) has a finer vertical (100-levels) and spatial (45km) resolution that may improve somewhat on the retrieval of lower tropospheric humidity and temperature. In addition, the latest version of AIRS (V6.28, to be released publically in V7 in 2017) shows some improvements related to humidity retrieval that are due to improved IR channel sampling. However, any major improvements in space-based CTP-HI retrieval and vertical resolution must come with next-generation satellite missions dedicated to retrieving PBL profiles.

Given the large sample of days required by the CDI, it is likely that the bulk signal of the CTP and HI and its relative variability over the 9+year period will still provide a self-consistent representation of dry and wet coupling regimes and variability. Figure 3 bears this out, and suggests that despite the scatter, there are still decent correlations in CTP and HI that can be exploited to represent dry vs. wet regimes. Likewise, the large scatter in SM should not prohibit the SM data from being representative of dry vs. wet regimes and surface conditions. Combining the CTP, HI and SM to identify areas of dry and wet coupling, the in-situ classification has a high consistency with the reanalysis while satellite observations have the lowest consistency (Fig. 4). This is not surprising given that MERRA and CFSR showed the highest correlations

with in-situ data of CTP, HI and SM (Fig. 3). Although there is a lack of consistency in the exact location of the dry and wet coupling regimes within the CTP-HI space across all the datasets, all the datasets, including satellite, indicate similar shapes and relative locations of the regimes. This indicates that all datasets show the existence of these regimes. This is particularly a novel finding of this study since this work represents the first time that in-situ observations have been applied to the Roundy et al. coupling classification. The in-situ and satellite remote sensing CDI provides a unique combination of observations that allows for an evaluation of model data at local and large scales that could be exploited in future studies. It is important to note that the in-situ comparisons are only valid at a single point over the SGP. While the SGP is an ideal location to have such in-situ observations, it would be ideal to compare in-situ data from other areas with satellite remote sensing. It is expected that in mountainous, perpetually cloudy, and cold regions it is unlikely to retrieve profiles as well down to the surface. However, this is a promising start, and indicates that satellite data (despite its limitations) can provide the information needed for such complex metrics as the CDI.

Applying the classification of the CTP-HI space to daily classification of the coupling state and the calculation of the CDI indicated similar results in that the in-situ CDI showed the strongest consistency with MERRA, however the monthly CDI from satellite still had a temporal correlation of 0.68 with the in-situ observations (Fig. 5a and b). Furthermore, the spatial patterns of CDI for satellite remote sensing are consistent with the reanalysis for June 2007 over the U.S. This indicates that both temporal and spatial patterns are largely captured by the CDI from satellite remote sensing and further demonstrates the potential of the AQUA dataset. There is however, a smaller magnitude both in space and in time in the CDI compared to the reanalysis. The lower magnitude CDI is especially noticeable during wet coupling as indicated in Fig. 5a

and c. This limitation could be partially due to missing values in the record, particularly during the wet coupling regime when there is more cloud cover that can limit the satellite observations. Missing values make the CDI move closer to zero, since it has the potential to reduce the numerator but not change the denominator in calculating the CDI. Future work will explore a revised CDI that would be less impacted by cloud cover and more relevant for satellite application. The limitation in the CDI magnitudes could also be partially due to the lack of resolution in the vertical from the atmospheric observations from satellite as shown in Fig. 2 along with difficulties in observing atmospheric humidity. It is hoped that through improvements in instruments and algorithms the quality of the satellite data will be increased and this limitation can be overcome.

Notwithstanding the shortcomings of the satellite data, it still has the potential to yield useful information as a large-scale observational record. As compared to other variables the CDI has the strongest correlation with the CTP and HI, from which it is derived, but also has strong correlation with VPD and DAT. These correlations are the highest over the U.S. during the summertime when land-atmosphere feedbacks play a stronger role in the evolution of the daytime temperature and humidity. The CDI also has a reasonable correlation with BLH. The correlations between CDI and the various variables were also lower when comparing satellite CDI to reanalysis variables as compared to reanalysis CDI. This is not surprising as there should be a level of consistency between the variables from the same reanalysis product. The results indicate that the CDI has the strongest relationship with atmospheric variables (DAT and VPD) that are greatly influenced by the land surface heat fluxes, e.g. sensible and latent heat fluxes, however it is not extensively correlated with any one variable and has its own unique characteristics. These unique characteristics could make it a useful drought-monitoring tool as it

has the potential to integrate multiple drivers and impacts of drought that may be missed by indices typically utilized for drought monitoring.

Overall this work demonstrates that there is sufficient information in the simultaneous measurements of the land and atmosphere from satellite remote sensing to provide useful information to the applications of drought monitoring and coupling metrics that can be used to evaluate GCMs. While it is recognized that the variables and metrics currently available through satellite remote sensing are not always the optimal choice for L-A coupling metrics, it is hoped that through further development, satellite based CDI can be utilized to provide new insights and application relevant for drought monitoring and prediction.

5. Acknowledgements

This research was partially supported by an appointment to the NASA Postdoctoral Program at the Goddard Space Flight Center, administered by Oak Ridge Associated Universities. Data were obtained from the Atmospheric Radiation Measurement (ARM) Program sponsored by the U.S. Department of Energy, Office of Science, Office of Biological and Environmental Research, Climate and Environmental Sciences Division. This financial and data support is gratefully acknowledged.

6. References

Betts, A. K., 1992: FIFE atmospheric boundary layer budget methods. *J. Geophys. Res.*, **97**, 18523, doi:10.1029/91JD03172. http://doi.wiley.com/10.1029/91JD03172 (Accessed January 19, 2016).

Dirmeyer, P. A., Z. Wang, M. J. Mbuh, and H. E. Norton, 2014: Intensified land surface control on boundary layer growth in a changing climate. *Geophys. Res. Lett.*, **41**, 2013GL058826, doi:10.1002/2013GL058826. http://dx.doi.org/10.1002/2013GL058826.

Ek, M. B., K. E. Mitchell, Y. Lin, E. Rogers, P. Grunmann, V. Koren, G. Gayno, and J. D. Tarpley, 2003: Implementation of Noah land surface model advances in the National Centers for Environmental Prediction operational mesoscale Eta model. *J. Geophys. Res.*, **108**, 16, doi:885110.1029/2002jd003296.

595 Ferguson, C. R., and E. F. Wood, 2011: Observed Land-Atmosphere Coupling from Satellite
596 Remote Sensing and Reanalysis. *J. Hydrometeorol.*, **12**, 1221–1254,
597 doi:10.1175/2011jhm1380.1.

598 Findell, K. L., and E. A. B. Eltahir, 2003a: Atmospheric controls on soil moisture-boundary layer
599 interactions. Part I: Framework development. *J. Hydrometeorol.*, **4**, 552–569,
600 doi:10.1175/1525-7541(2003)004<0552:acosml>2.0.co;2.

601 ——, and ——, 2003b: Atmospheric controls on soil moisture-boundary layer interactions. Part
602 II: Feedbacks within the continental United States. *J. Hydrometeorol.*, **4**, 570–583,
603 doi:10.1175/1525-7541(2003)004<0570:acosml>2.0.co;2.

604 Findell, K. L., P. Gentine, B. R. Lintner, and C. Kerr, 2011: Probability of afternoon
605 precipitation in eastern United States and Mexico enhanced by high evaporation. *Nat.*
606 *Geosci*, **advance on**. http://dx.doi.org/10.1038/ngeo1174.

607 Koster, R. D., M. J. Suarez, A. Ducharne, M. Stieglitz, and P. Kumar, 2000: A catchment-based
608 approach to modeling land surface processes in a general circulation model 1. Model
609 structure. *J. Geophys. Res.*, **105**, 24809–24822, doi:10.1029/2000jd900327.

610 ——, and Coauthors, 2006: GLACE: The Global Land-Atmosphere Coupling Experiment. Part
611 I: Overview. *J. Hydrometeorol.*, **7**, 590–610, doi:10.1175/jhm510.1.

612 Lintner, B. R., P. Gentine, K. L. Findell, and G. D. Salvucci, 2014: The Budyko and
613 complementary relationships in an idealized model of large-scale land–atmosphere
614 coupling. *Hydrol. Earth Syst. Sci. Discuss.*, **11**, 9435–9473, doi:10.5194/hessd-11-9435-
615 2014. http://www.hydrol-earth-syst-sci-discuss.net/11/9435/2014/hessd-11-9435-2014.html
616 (Accessed May 11, 2015).

617 Owe, M., R. de Jeu, and T. Holmes, 2008: Multisensor historical climatology of satellite-derived
618 global land surface moisture. *J. Geophys. Res. Surf.*, **113**, 17,
619 doi:F0100210.1029/2007jf000769.

620 Rienecker, M. M., and Coauthors, 2011: MERRA: NASA's Modern-Era Retrospective Analysis
621 for Research and Applications. *J. Clim.*, **24**, 3624–3648, doi:10.1175/jcli-d-11-00015.1.
622 http://dx.doi.org/10.1175/JCLI-D-11-00015.1.

623 Roundy, J. K., and E. F. Wood, 2014: The Attribution of Land–Atmosphere Interactions on the
624 Seasonal Predictability of Drought. *J. Hydrometeorol.*, **16**, 793–810, doi:10.1175/JHM-D-
625 14-0121.1. http://dx.doi.org/10.1175/JHM-D-14-0121.1.

626 ——, C. R. Ferguson, and E. F. Wood, 2013a: Temporal Variability of Land–Atmosphere
627 Coupling and Its Implications for Drought over the Southeast United States. *J.*
628 *Hydrometeorol.*, **14**, 622–635, doi:10.1175/JHM-D-12-090.1.
629 http://dx.doi.org/10.1175/JHM-D-12-090.1.

630 ——, C. Ferguson, and E. Wood, 2013b: Impact of land-atmospheric coupling in CFSv2 on
631 drought prediction. *Clim. Dyn.*, 1–14, doi:10.1007/s00382-013-1982-7.
632 http://dx.doi.org/10.1007/s00382-013-1982-7.

633 Saha, S., and Coauthors, 2010: The NCEP Climate Forecast System Reanalysis. *Bull. Am.*
634 *Meteorol. Soc.*, **91**, 1015–1057, doi:10.1175/2010bams3001.1.
635 http://dx.doi.org/10.1175/2010BAMS3001.1.

636 ——, and Coauthors, 2014: The NCEP Climate Forecast System Version 2. *J. Clim.*,

637 doi:10.1175/JCLI-D-12-00823.1. http://dx.doi.org/10.1175/JCLI-D-12-00823.1.

638 Santanello, J. A., C. D. Peters-Lidard, S. V Kumar, C. Alonge, and W.-K. Tao, 2009: A
639 Modeling and Observational Framework for Diagnosing Local Land-Atmosphere Coupling
640 on Diurnal Time Scales. *J. Hydrometeorol.*, **10**, 577–599, doi:10.1175/2009jhm1066.1.

641 Santanello, J. A., and Coauthors, 2011: Local land-atmosphere coupling (LoCo) Research: Status
642 and Results. *GEWEX Newsl.*, **21**, 7–9.

643 Santanello, J. A., C. D. Peters-Lidard, A. Kennedy, and S. V Kumar, 2013: Diagnosing the
644 Nature of Land–Atmosphere Coupling: A Case Study of Dry/Wet Extremes in the U.S.
645 Southern Great Plains. *J. Hydrometeorol.*, **14**, 3–24, doi:10.1175/JHM-D-12-023.1.
646 http://dx.doi.org/10.1175/JHM-D-12-023.1.

647 ——, J. Roundy, and P. A. Dirmeyer, 2015: Quantifying the Land–Atmosphere Coupling
648 Behavior in Modern Reanalysis Products over the U.S. Southern Great Plains. *J. Clim.*, **28**,
649 5813–5829, doi:10.1175/JCLI-D-14-00680.1. http://dx.doi.org/10.1175/JCLI-D-14-
650 00680.1.

651 Seneviratne, S. I., T. Corti, E. L. Davin, M. Hirschi, E. B. Jaeger, I. Lehner, B. Orlowsky, and A.
652 J. Teuling, 2010: Investigating soil moisture–climate interactions in a changing climate: A
653 review. *Earth-Science Rev.*, **99**, 125–161, doi:10.1016/j.earscirev.2010.02.004.
654 http://www.sciencedirect.com/science/article/pii/S0012825210000139 (Accessed July 14,
655 2014).

656 Song, H.-J., C. R. Ferguson, and J. K. Roundy, 2015: Land-atmosphere coupling at the Southern
657 Great Plains Atmospheric Radiation Measurement (ARM) field site and its role in
658 anomalous afternoon peak precipitation. *J. Hydrometeorol.*, 151019113236006,
659 doi:10.1175/JHM-D-15-0045.1. http://journals.ametsoc.org/doi/abs/10.1175/JHM-D-15-
660 0045.1 (Accessed October 26, 2015).

661 Stommel, H., 1947: ENTRAINMENT OF AIR INTO A CUMULUS CLOUD. *J. Meteorol.*, **4**,
662 91–94, doi:10.1175/1520-0469(1947)004<0091:EOAIAC>2.0.CO;2.
663 http://journals.ametsoc.org/doi/abs/10.1175/1520-
664 0469(1947)004%3C0091%3AEOAIAC%3E2.0.CO%3B2 (Accessed January 19, 2016).

665 Susskind, J., J. M. Blaisdell, L. Iredell, and F. Keita, 2011: Improved Temperature Sounding and
666 Quality Control Methodology Using AIRS/AMSU Data: The AIRS Science Team Version
667 5 Retrieval Algorithm. *Ieee Trans. Geosci. Remote Sens.*, **49**, 883–907,
668 doi:10.1109/tgrs.2010.2070508.

669 Tawfik, A. B., P. A. Dirmeyer, and J. A. Santanello, 2015: The Heated Condensation
670 Framework. Part I: Description and Southern Great Plains Case Study. *J. Hydrometeorol.*,
671 150603105509002, doi:10.1175/JHM-D-14-0117.1.
672 http://journals.ametsoc.org/doi/abs/10.1175/JHM-D-14-0117.1 (Accessed June 8, 2015).

673 Taylor, C. M., R. A. M. de Jeu, F. Guichard, P. P. Harris, and W. A. Dorigo, 2012: Afternoon
674 rain more likely over drier soils. *Nature*, **489**, 423–426.
675 http://dx.doi.org/10.1038/nature11377.

676

677

678

679

Table Caption List

Table 1. A summary of the relative the relative characteristics from each dataset used to derive the CDI.

Figure Caption List

Figure 1. The basis for the coupling regime classification method (Roundy et al., 2013) where a) is an example of the three variables (CTP, HI, SM) used in the coupling classification and the resulting classification of the CTP-HI space based on Soil Moisture (SM) with b) an example of a dry and wet coupling event for a point (36.5°N, 97.5°W) in the Southern Great Plains in the U.S based on data from the MERRA reanalysis.

Figure 2. The atmospheric profile and corresponding CTP and HI at 07:30 UTC AQUA (peach) and 05:30 UTC in-situ (red) for a day during a) a dry year (2006-06-07) and b) a wet year (2007-06-03) for the Southern Great Plains location (36.5°N, 97.5°W).

Figure 3. Comparison of the a) CTP, b) HI and c) SM from satellite remote sensing (AQUA) and reanalysis (MERRA, CFSR) with in-situ observations for a point in the Southern Great Plains (36.5°N, 97.5°W) for the available data from 2003-2015. The regression line (red), Pearson correlation (rp) and Spearman correlation (rs) are also given.

Figure 4. The classified CTP-HI space from in-situ observations, satellite (AQUA) and reanalysis (MERRA, CFSR) for a point in the Southern Great Plains (36.5°N, 97.5°W). The percent consistent of each coupling regime as compared to in-situ observations is also given.

Figure 5. Comparison of In-situ CDI with reanalysis (MERRA and CFSR) and satellite remote sensing (AQUA) for a point in the Southern Great Plains (36.5°N, 97.5°W) for a) Monthly Timeseries from 2003-2015, b) scatter plots of the monthly values for May through September

with the dark gray points from 2003-2011 and the light gray from 2012-2015 and c) the spatial variability of the CDI in June 2007. The regression line (red), Pearson correlation (rp) and Spearman correlation (rs) are also given in b).

Figure 6. The monthly standardized anomaly Spearman correlation (2003-2015) of the CDI with Precipitation (P), Total Soil moisture (TSM), Daytime Average Temperature (DAT), Vapor Pressure Deficit (VPD), Evaporative Fraction (EF), Boundary Layer Height (BLH), Convective Triggering Potential (CTP) and Humidity Index (HI) for CDI from AQUA and other variables from MERRA (Top), AQUA CDI and CFSR variables (Middle) and MERRA CDI and MERRA variables (Bottom) for climate regions of the U.S. (colored shapes) and the average over the U.S. plotted as boxes reflected around zero. The horizontal red dashed lines indicate statistical significance at $p = 0.05$ for the monthly values from May-Sep ($r = 0.24$) and all the monthly values significance ($r = 0.16$).

721 Table 1. A summary of the relative the relative characteristics from each dataset used to derive

722 the CDI.

Dataset	***Type***	***Spatial Coverage***	***Atmospheric Levels***	***Variables***	***Temporal Range***
AQUA	Satellite	Global	**12**	**CTP-HI**: AIRS **SM**: AMSR-E	2003-2015 2003-2011
MERRA	Reanalysis	Global	**72**	**CTP-HI**: MERRA **SM**: MERRA	1979-2015
CFSR	Reanalysis	Global	**64**	**CTP-HI**: CFSR SM: CFSR	1979-2015
In-situ	Observations	Point: ARM Central Facility, Lamont OK	**> 1000**	**CTP-HI**: Radiosonde **SM**: SWATS	2003-2015

723

724

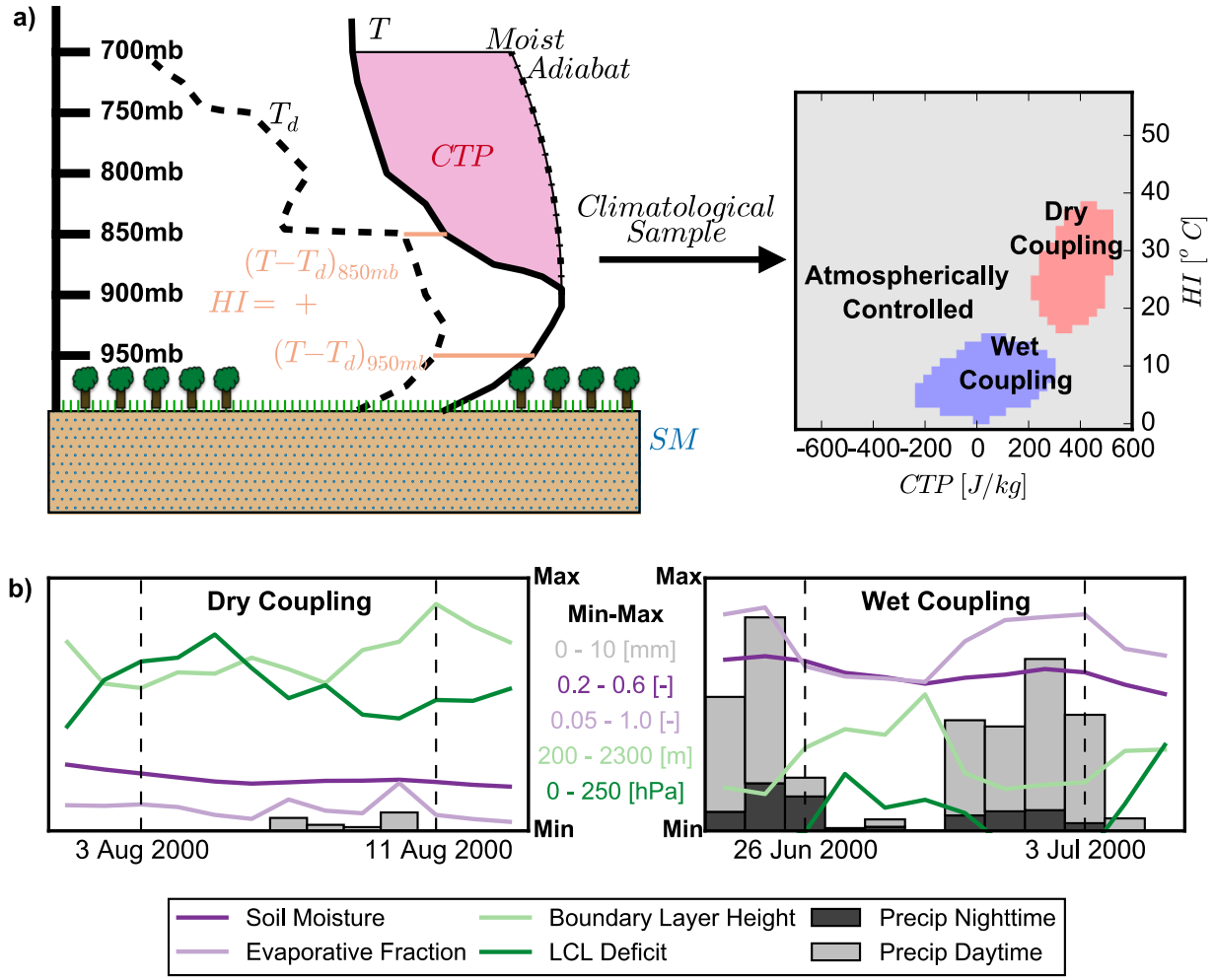

Figure 1. The basis for the coupling regime classification method (Roundy et al., 2013) where a) is an example of the three variables (CTP, HI, SM) used in the coupling classification and the resulting classification of the CTP-HI space based on Soil Moisture (SM) with b) an example of a dry and wet coupling event for a point (36.5°N, 97.5°W) in the Southern Great Plains in the U.S based on data from the MERRA reanalysis.

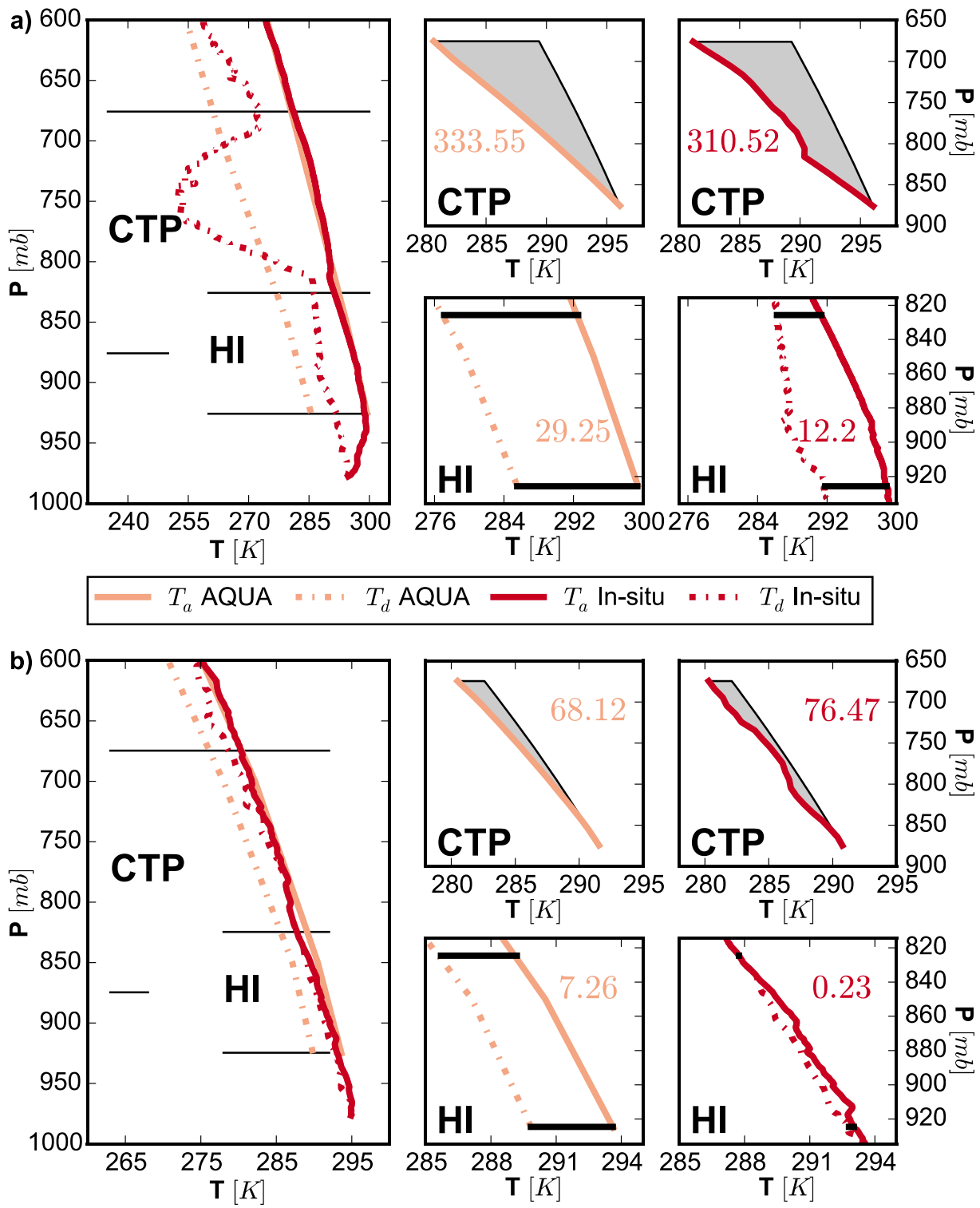

Figure 2. The atmospheric profile and corresponding CTP and HI at 07:30 UTC AQUA (peach) and 05:30 UTC in-situ (red) for a day during a) a dry year (2006-06-07) and b) a wet year (2007-06-03) for the Southern Great Plains location (36.5°N, 97.5°W).

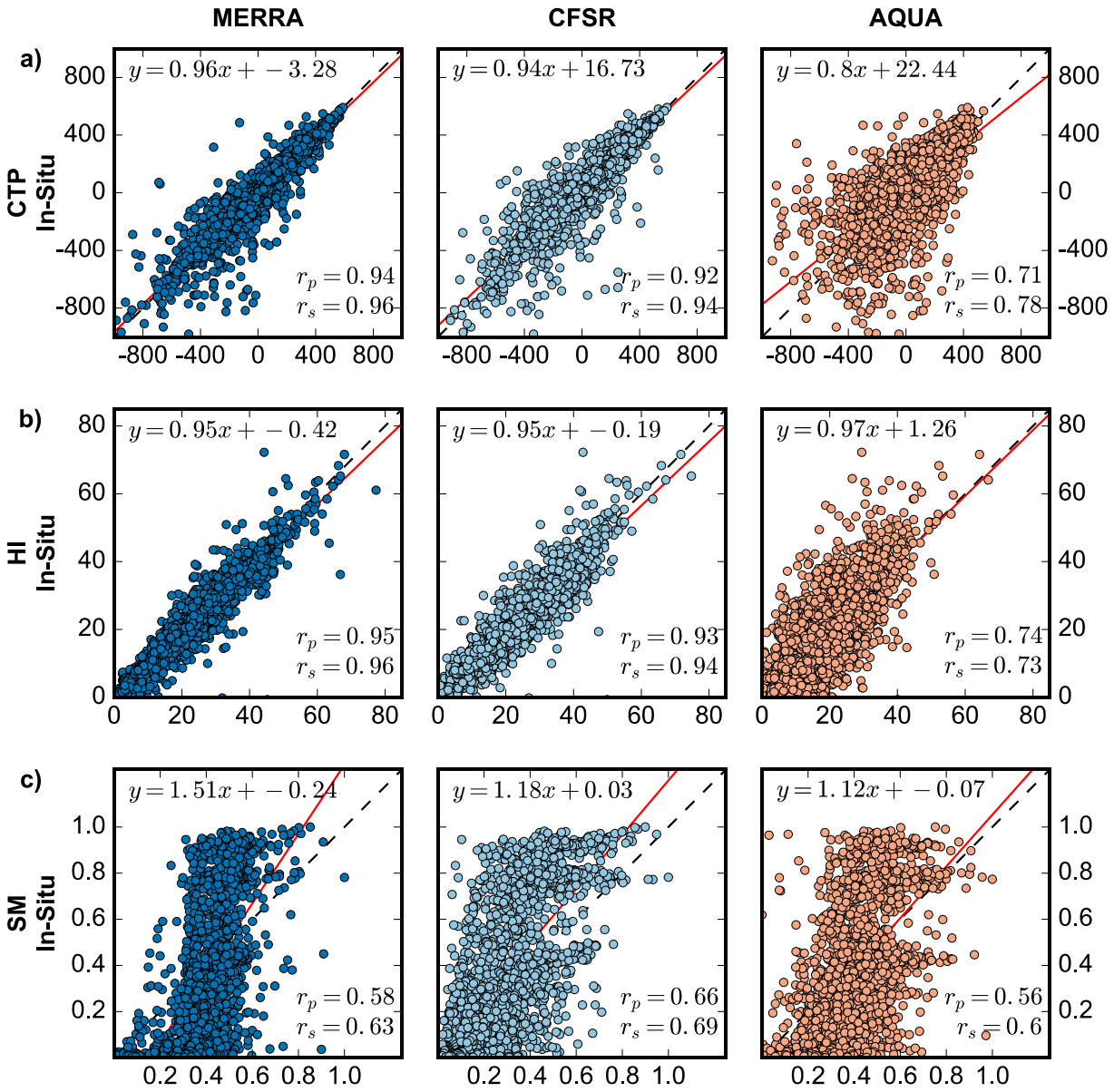

Figure 3. Comparison of the a) CTP, b) HI and c) SM from satellite remote sensing (AQUA) and reanalysis (MERRA, CFSR) with in-situ observations for a point in the Southern Great Plains (36.5°N, 97.5°W) for the available data from 2003-2015. The regression line (red), Pearson correlation (r_p) and Spearman correlation (r_s) are also given.

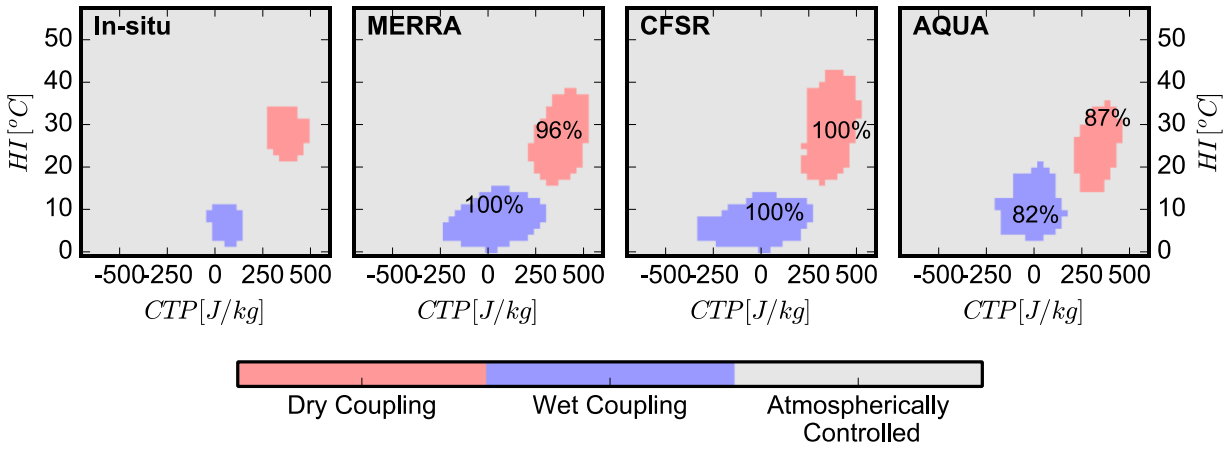

743

744 Figure 4. The classified CTP-HI space from in-situ observations, satellite (AQUA) and

745 reanalysis (MERRA, CFSR) for a point in the Southern Great Plains (36.5°N, 97.5°W). The

746 percent consistent of each coupling regime as compared to in-situ observations is also given.

747

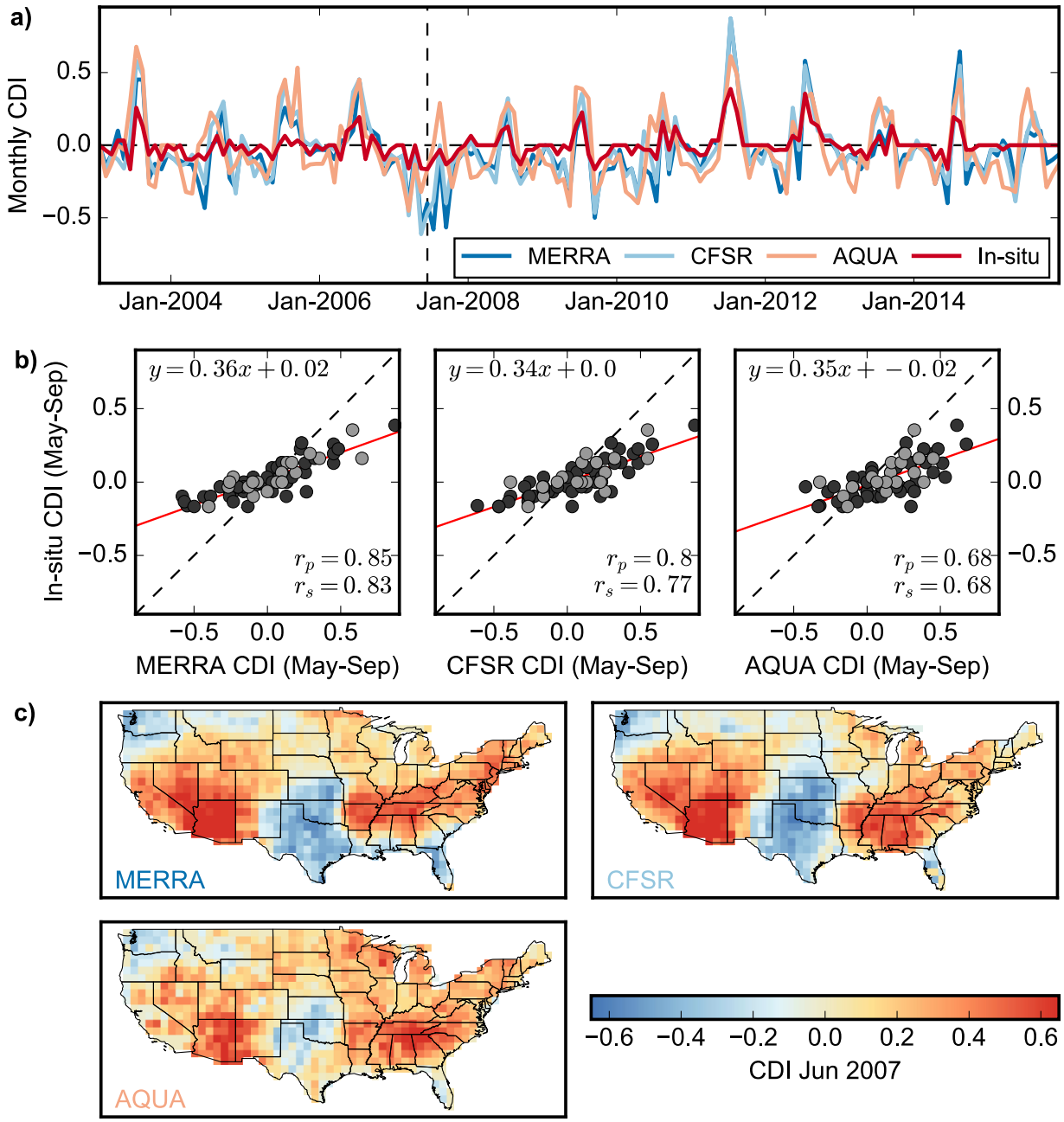

Figure 5. Comparison of In-situ CDI with reanalysis (MERRA and CFSR) and satellite remote sensing (AQUA) for a point in the Southern Great Plains (36.5°N, 97.5°W) for a) Monthly Timeseries from 2003-2015, b) scatter plots of the monthly values for May through September with the dark gray points from 2003-2011 and the light gray from 2012-2015 and c) the spatial

753 variability of the CDI in June 2007. The regression line (red), Pearson correlation (r_p) and

754 Spearman correlation (r_s) are also given in b).

755

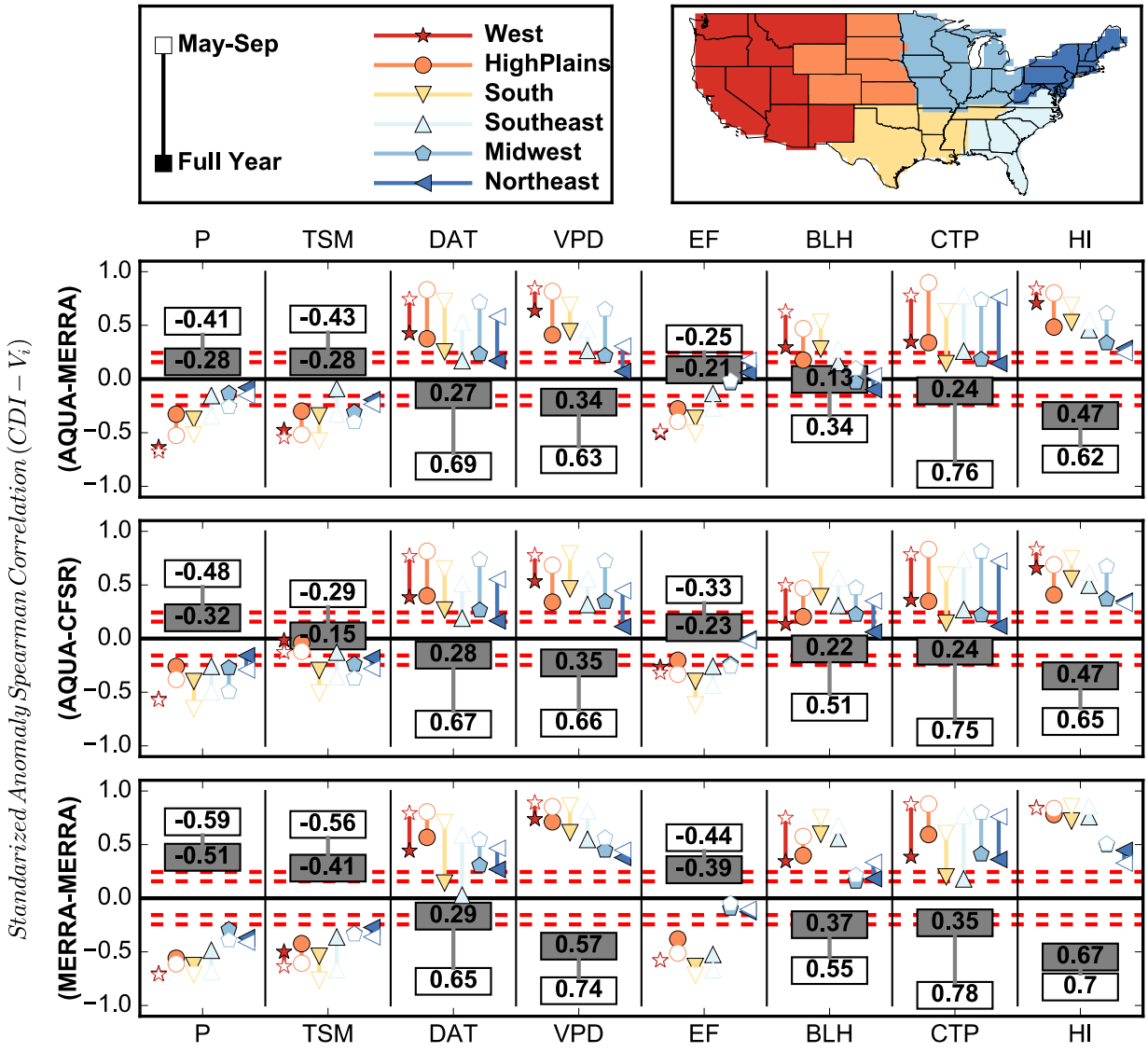

Figure 6. The monthly standardized anomaly Spearman correlation (2003-2015) of the CDI with Precipitation (P), Total Soil moisture (TSM), Daytime Average Temperature (DAT), Vapor Pressure Deficit (VPD), Evaporative Fraction (EF), Boundary Layer Height (BLH), Convective Triggering Potential (CTP) and Humidity Index (HI) for CDI from AQUA and other variables from MERRA (Top), AQUA CDI and CFSR variables (Middle) and MERRA CDI and MERRA variables (Bottom) for climate regions of the U.S. (colored shapes) and the average over the U.S. plotted as boxes reflected around zero. The horizontal red dashed lines indicate statistical

764 significance at p = 0.05 for the monthly values from May-Sep (r = 0.24) and all the monthly

765 values significance (r = 0.16).